Reducing indoor particle exposure using mobile air purifiers—Experimental and numerical analysis

Cite as: AIP Advances 11, 125114 (2021); doi: 10.1063/5.0064805
Submitted: 27 July 2021 • Accepted: 7 November 2021 •
Published Online: 9 December 2021

Adrian Tobisch,[1] Lukas Springsklee,[1,a)] Lisa-Franziska Schäfer,[2] Nico Sussmann,[2] Martin J. Lehmann,[3] Frederik Weis,[4] Raoul Zöllner,[2] and Jennifer Niessner[1]

AFFILIATIONS

[1] Institute of Flow in Additively Manufactured Porous Media (ISAPS), Heilbronn University of Applied Sciences, Max-Planck-Str. 39, 74081 Heilbronn, Germany
[2] Institute of Automotive Engineering and Mechatronics (IKM), Heilbronn University of Applied Sciences, Max-Planck-Str. 39, 74081 Heilbronn, Germany
[3] MANN+HUMMEL GmbH, Schwieberdinger Straße 126, 71636 Ludwigsburg, Germany
[4] Palas GmbH, Greschbachstrasse 3b, 76229 Karlsruhe, Germany

[a)] **Author to whom correspondence should be addressed:** lukas.springsklee@hs-heilbronn.de

ABSTRACT

Aerosol particles are one of the main routes of transmission of COVID-19. Mobile air purifiers are used to reduce the risk of infection indoors. We focus on an air purifier that generates a defined volumetric air flow through a highly efficient filter material. We investigate the transport of aerosol particles from an infected dummy equipped with an aerosol generator to receiving thermal dummies. For analysis, we use up to 12 particle sensors to monitor the particle concentration with high spatial resolution. Based on the measurement data, a computational fluid dynamics (CFD) model is set up and validated. The experimental and numerical methods are used to investigate how the risk of infection suggested by the particle exposure in an exemplary lecture hall can be reduced by a clever choice of orientation of the air purifier. It turns out that obstructing the outlet stream of the air purifier may be particularly advantageous. The particle concentration at the head height deviates by 13% for variations of the location and orientation. At an air change per hour of 5, the cumulated PM1 mass at the head level was reduced by 75%, independently of the location of the infected dummy, compared to the "natural decay" case, showing that filtration is an effective means of reducing aerosol particle concentrations. Finally, CFD simulation was used to monitor the particle fates. The steady simulation results fit quite well with the experimental findings and provide additional information about the particle path and for assessing the comfort level due to air flow.

I. INTRODUCTION

The COVID-19 pandemic has implied large restrictions to public and private life and has far-reaching effects on society, culture, science, and the economy. It is well known that a major route of infection with SARS-CoV-2 is the transmission by aerosol-borne viral pathogens.[1] These virus-laden aerosols may be emitted when talking, shouting, singing, coughing, sneezing, or simply breathing. Small aerosol particles may remain suspended in the air for hours.[2] Infections may occur by proximity when aerosols emitted by one person are directly transported toward another person. On top of this direct infection route via droplets, an indirect infection route exists indoors where the aerosol particle concentration, and thus infection risk, increases with time depending on the number of persons present, their activity, and the air volume within the room.[3] Since people spend over 90% of their time indoors and several persons may be infected at a time, indoor situations are most crucial for SARS-CoV-2 transmission.[4] Personal protective measures, such as masks, will never be able to remove all particles; therefore, ventilation is of utmost importance as an additional measure. While opening windows very regularly (if possible) is helpful under warm conditions, air filtration is an important supplement in spring, autumn,

and winter. Discussions about ventilation strategies by opening windows, the use of face masks during class, lectures, or office work, and the possible risk of infection are numerous. Understanding and controlling aerosols seem to be the key mechanism to minimize the infection risks. In this context, computational fluid dynamics (CFD) modeling is a powerful tool to investigate aerosol particle transport and fate. In addition, recent advances in sensor network technology provide the possibility not only to measure particle concentrations at a few locations within a room but also to monitor the aerosol particle concentration as a measure of infection risk at the locations where particles are potentially inhaled.

While the infection risk through air borne transmission is dependent on multiple factors, mainly the number of emitted virus-laden particles, the half-life of the virus, and the number of inhaled viable viruses, lowering the concentration of virus-laden particles in the air is key to lowering the infection risk of occupants via the indirect infection route indoors.[5] This can be achieved by either diluting the air with virus-free fresh air or by removing the aerosol particles using highly efficient filters. While critical places, such as operating rooms, achieve this through Heating, Ventilation, and Air Conditioning (HVAC) systems with air changes per hour (ACHs) ranging from 15 to 40[6], most HVAC systems in classrooms, theaters, and offices are not designed to reduce the infection risk but rather to keep the CO_2 concentration below the recommended level of 1000 ppm.[7]

Mobile air purifiers represent a chance to reduce the aerosol particle concentration by removing particles from the air using highly efficient filters.[8] For this purpose, ACHs of 5–6 are recommended.[6,9] Multiple studies have investigated the decay rates of the aerosol particle concentration using air purifiers at varied ACHs. Burgmann and Janoske[10] showed that at an ACH of 6, the aerosol particle concentration is reduced by ~80% within 30 min. Kähler *et al.* reported decay rates ranging from 1.5 to 3.8 h^{-1}, resulting in half-life times between 10 and 27 min depending on the ACH. In order to minimize the dwell time of the aerosol particles, Kähler *et al.* recommended placing the air purifier in the center of the room if possible.[9] Curtius *et al.* were able to report a 95% reduction in the aerosol particle concentration after 37 min using multiple purifiers to obtain the recommended ACH of 5. The decay rate determined at an ACH of 5.7 was $(0.107 \pm 0.01)\ min^{-1}$, while the natural decay rate was $(0.020 \pm 0.01)\ min^{-1}$.[11]

Since the air velocity is larger at the outlet than at the intake, the purified air is discharged at a greater distance.[12] On account that aerosol particles move with bulk air, this presents a chance for the air purifier to disperse the aerosol particles throughout the room, rather than removing them.[13] Küpper *et al.* showed that the clean air delivery rate (CADR) of an air purifier in a small room of 70 m^3 is largely independent of its position. By placing the air purifier in a particular disadvantageous position, the decay rate of the particle concentration and therefore the CADR decreased.[14]

The CADR is determined from Eq. (1) by measuring the reduction rate $k_{purifier}$ of aerosol particles (particle size ranging from 0.09 to 11 μm) taking the natural decay rate $k_{natural}$ into account in a standardized test chamber V_{room},[15] while the ACH is calculated using the volumetric flow rate of the air purifier divided by the room volume. This entails that although the ACH of a particular air purifier is in line with recommendations, the CADR can be greatly reduced by a disadvantageous installation,

$$CADR = (k_{purifier} - k_{natural}) \cdot V_{room}. \quad (1)$$

The investigation of the effectiveness of air purifiers in reducing the indoor aerosol particle concentration often combines experimental and numerical methods. This allows for the examination of multiple cases using validated CFD models while minimizing experimental effort. Multiple studies have modeled the transport of aerosol particles indoors. In these publications, various results of the importance of humidity and the thermal effects to a numerical particle simulation are discussed.

Feng *et al.*[1] showed that most numerical studies report that condensation and evaporation due to humidity have a negligible effect on the particle distribution. Chen *et al.*[16] and Farkas *et al.*[17] focused on the deposition of multicomponent droplets and evaporation in a human respiratory tract. Feng *et al.*[1] faced this question of humidity and evaporation effects in indoor conditions, like in this study of a lecture hall. Xie *et al.*[18] showed that the evaporation time of water aerosols with a diameter of a few micrometers is less than one second. In preliminary simulation studies, this effect has been confirmed by the authors using ANSYS Fluent. Mutuku *et al.*[19] investigated different turbulence models and solver algorithms for particle simulations. In most studies, an Euler–Lagrange method is used to simulate a multiphase particle flow.[20] Due to the low mass loading, a one-way coupling is used for fluid particle interactions.[21] Regarding the continuous phase, it can be assumed that an indoor air flow is incompressible and turbulent.[10]

For turbulence modeling, Abuhegazy *et al.*[21] used a $k - \varepsilon$ model following the Reynolds-averaged Navier–Stokes equation (RANS) approach since the time-averaged results are often of interest. Modeling the discrete phase, the particle diameter distribution is important for the simulation.[19] Brownian particular motion can be neglected because the particle diameters are still too large.[21] In the simulation of air purifiers using highly efficient particle filters (HEPA class H13 and higher), it can be assumed that 100% of the particles get removed.[10]

In contrast to this study in a lecture hall, Dbouk and Drikakis[20] investigated aerosol dispersion in very confined spaces as in an elevator and pointed out that the location of the inlets and outlets has a significant influence on the aerosol distribution. A larger outdoor environment is investigated by Gorbunov[22] who showed in a simulation that aerosol particles can travel over a distance of 30 m. Bathula *et al.*[23] used simulation to investigate how long infectious particles remain in a room. This has practical implication regarding the safety of medical staff. Pyankov *et al.*[24] presented a study of time-dependent inactivation of MERS-CoV in ambient air under climatic conditions representing a common office environment. An alternative way of reducing infection risk is to inactivate the virus rather than removing aerosol particles. Rezaei *et al.*[25] investigated virus elimination by heat in air conditioning systems to reduce the amount of contaminated particles.

Another study on virus inactivation by UV-C irradiation is investigated by using numerical simulations of virus-laden droplets.[26] However, particles are still contaminated on the path from the source to the air cleaner, like when using common filtrating air purifiers.

The literature review shows investigations of the general dispersion of aerosols in different rooms and under different conditions. However, the studies do not focus on the particle load that

the persons are exposed to at their seat positions. Consequently, in this study, we investigate the particle concentration at positions where particles may be inhaled by persons using a high spatial resolution.

Therefore, the purpose of this work is given as follows:

- To assess the influence of the position and the orientation of an air purifier on the aerosol particle concentration within the room and to identify preferable cases.
- To investigate the particle exposure of persons by measuring particle concentrations using a sensor network consisting of 12 PM1 sensors exactly at the locations where particles may be inhaled.
- To include the influence of thermal buoyancy by mimicking the effect of persons present in the room using "thermal dummies".
- To investigate particle concentrations for the case that a sink (air purifier) fights against a source (infected person) and by studying commonly considered decay.
- To validate a CFD model based on the measurements in order to (1) increase process understanding by allowing for a visualization of the flow field in a room and (2) allow for the investigation of situations that can hardly or not be considered experimentally.

In Sec. II, we give an overview on the situation in the lecture hall considered, the experimental material, and the setup. Next, in Sec. III, we introduce the mathematical and numerical models and give an overview on the considered cases. The numerical model is validated in Sec. IV, and both numerical and experimental results are presented and discussed. Finally, we sum up and give an outlook on future research in Sec. VI.

II. SITUATION AND EXPERIMENTAL SETUP

Experiments were performed in a lecture hall at the Heilbronn University of Applied Sciences. The dimension of the room is 11 × 8.5 × 3 m. Due to the ascending rows, the ceiling height in the back of the room is significantly lower, resulting in a room volume of ~250 m^3. The room provides seating for up to 80 students and one professor. The total window area is 20 m^2, of which 6 m^2 can be used for ventilation.

The HVAC system is turned off during the entirety of the experiments. The room is equipped with a portable air purifier (SQ 2500, MANN + HUMMEL) capable of a maximum volumetric air flow of 2500 m^3/h, delivering a maximum theoretical ACH of 10. The air purifier is fitted with an HEPA H14 filter that gets removed at minimum 99 975% of particles at the most penetrating particle size (MPPS).[27] The intake is located at the front side and has an area of 0.32 m^2. The outlet is on a side of the device adjacent to this front side and has an area of 0.28 m^2. The air flow of the device is denoted by the arrows seen in Fig. 1 (left). Up to nine thermal dummies are deployed to simulate the heat flux contribution of persons in the room, in addition to serving as obstacles for the flow. The dummies are made of cardboard equipped with light bulbs emitting a thermal energy of ~75 W in accordance with the thermal contribution of students in a lecture scenario specified by DIN EN 16798-1.[7] The room is equipped with up to 12 particle sensors, made up of four high-end optical particle counters (OPCs) (Fidas Frog, PALAS) and a network of eight low-cost photometric particle sensors (lcps) (SPS 30, SENSIRION). The temperature, ambient pressure, and relative humidity are measured at each point. Each device measures aerosol particles in the size range of 0.18–18 μm (Fidas Frog) or 0.3–10 μm (SPS 30). The high-end devices are deployed to measure particles at the table height, while the low-cost sensors are placed at the "face height" of the dummies. The aerosol particles are produced using an atomizer (AGK 2000, PALAS) with a sodium chloride solution. The emitted particle size distribution is adjusted via the mass concentration of the saline solution, while the mass flow is set through the applied compressed air pressure.

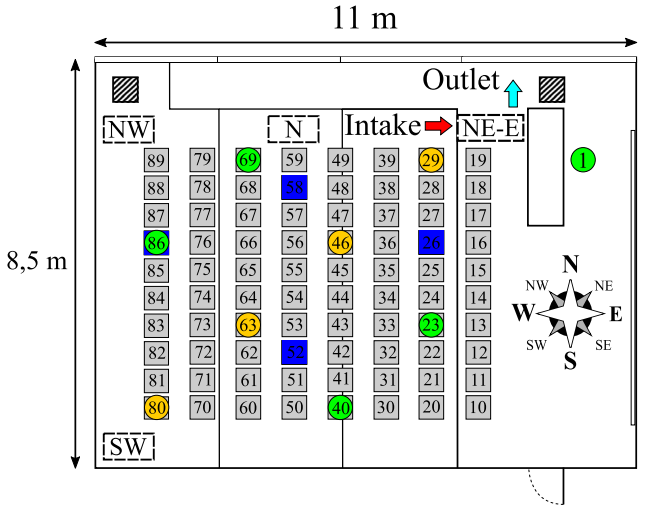

FIG. 1. Position of the air purifier, receiving and emitting thermal dummies (marked by green and orange circles), and high-end optical particle counters (OPCs) (marked blue).

A. Influence of the position, orientation, and flow rate

In the first experimental setup, the influence of the position, orientation, and flow rate of the air purifier on the spreading and degradation of the aerosol particle concentration is investigated. For this purpose, the aerosol particles are emitted in a fixed place in the center of the room using compressed air at 3.5 bars and a sodium chloride solution of 2.5 wt. %. The particle counters are positioned at the table height at the measurement points MP 26, MP 58, MP 86, and MP 52 (see Fig. 1). The experiments consist of two phases. In the first phase, the aerosol particles are emitted for a duration of 20 min, after which the atomizer is shut off and the decay of the particle concentration is monitored. The air purifier is positioned at four different locations throughout the room, and at each position, the orientation is varied so that the inlet and outlet point in different directions into the room or against an obstacle, in this case either the window front or the wall. If the outlet and/or intake are pointed at an obstacle (either the wall or window) at a distance of 0.3–1 m, they are considered to be obstructed, and if they point freely into the room, they are considered unobstructed.

The following positions are identified as viable places to set up the mobile air purifier (see Fig. 1):

- NE: North-East near the window panel;
- N: North near the window panel;
- NW: North-West near the window panel;
- SW: South-West near the wall.

At most locations, particular orientations are disqualified as viable setup options due to proximity to students or the professor, therefore likely exceeding air velocity limits for thermal comfort. The position and orientation of the air purifier are encoded using the cardinal direction relative to the compass seen in Fig. 1 to identify the location, appended by the air flow direction at the intake of the air purifier. This leaves the following cases for the experimental setup:

- NE-N and NE-E;
- N-E;
- NW-N, NW-W, NW-S, and NW-E;
- SW-N, SW-W, and SW-S.

The effectiveness of the operation parameters of the mobile air purifier (position and orientation) is evaluated by the numerical integration of the mass concentration of particles smaller than 1 μm (PM1 fraction) over the duration of the experiment. This is due to the fact that virus-laden droplet nuclei are known to be in a size regime <1 μm.[28] The value is then multiplied by $1.333 \cdot 10^{-4}$ m^3/s (8 L/min), representing the volume flow rate of a breathing person in a relaxed condition. This gives an average mass of PM1, which is inhaled at the measuring point over the duration of the experiment. Splitting up into the charging and decaying phases of the experiments, this value is used to identify the PM1 dose potentially inhaled at each measurement point throughout the classroom. By fitting the decay curve with an exponential decay function

$$C_{m,PM1}(t) = C_{m,0} \cdot e^{-k_{purifier}t}, \tag{2}$$

the decay rate $k_{purifier}$ at each measurement point is determined.

B. Influence of the particle source on local particle exposure

The second experimental setup focuses on the influence of the position of the aerosol particle source on the distribution and decay of particles for the fixed positions and orientation of the air purifier. Derived from the first experimental setup, the following three cases are identified for further investigation: SW-W, SW-N, and SW-S. These cases represent a corner installation with an obstructed outlet (SW-W), obstructed outlet and intake (SW-N), and unobstructed outlet and intake (SW-S). The fourth case is a reference case where the air purifier is turned off. Nine thermal dummies are positioned throughout the room at a maximum distance to each other, as shown in Fig. 1. The location of the aerosol particle source is varied. The aerosol particles were emitted at seats 29, 46, and 80. The particle concentration at the table height and "face-height" of the dummies is measured.

III. NUMERICAL SETUP

In addition to the experimental studies, numerical flow simulations are performed to achieve a deeper insight into the indoor air flow and the aerosol distribution. Additional cases are considered that can hardly be implemented in the experimental setup.

A. Numerical approach

Two different numerical approaches of multiphase flows have been established: Euler–Lagrange approach and Euler–Euler approach. In particle laden flows with a low mass loading, the Lagrangian approach is advantageous. It is assumed that a mass point approach with the approximation of the forces by particle volume is sufficient. Therefore, the particles are assumed to be spherical. Due to the low mass loading of less than 10%, an Euler–Lagrange approach with a discrete phase model (DPM) and a one-way-coupling is used for the numerical simulations. The continuous phase influences the discrete phase by friction and turbulence. However, the particles do not influence the flow.[29]

1. Governing equations for the Euler–Lagrange approach

Continuous phase: In this case, the flow field is calculated before the discrete phase calculation. Therefore, there is no influence of the particles on the flow field, and the classical Navier–Stokes equations are solved,[30]

$$\frac{\partial}{\partial t}\rho_F + \nabla \cdot (\rho_F \vec{u}) = 0, \tag{3}$$

$$\frac{\partial}{\partial t}(\rho_F \cdot \vec{u}) + \nabla \cdot (\rho_F \cdot \vec{u} \times \vec{u} + pI - \widetilde{\tau}) = \rho_F \cdot \vec{f}, \tag{4}$$

$$\frac{\partial}{\partial t}\left(\rho_F\left(e + \frac{\vec{u}^2}{2}\right)\right) + \nabla\left(\rho_F \vec{u} \cdot \left(h + \frac{\vec{u}^2}{2}\right) - (\widetilde{\tau} \cdot \vec{u}) - \lambda \nabla T\right) = \rho_F \vec{f} \vec{u}, \tag{5}$$

$$\vec{u} = \begin{bmatrix} u \\ v \\ w \end{bmatrix} \vec{f} = \begin{bmatrix} f_x \\ f_y \\ f_z \end{bmatrix} I = \begin{bmatrix} 1 & 0 & 0 \\ 0 & 1 & 0 \\ 0 & 0 & 1 \end{bmatrix} \widetilde{\tau} = \begin{bmatrix} \tau_{xx} & \tau_{xy} & \tau_{xz} \\ \tau_{yx} & \tau_{yy} & \tau_{yz} \\ \tau_{zx} & \tau_{zy} & \tau_{zz} \end{bmatrix}. \tag{6}$$

Index F represents fluid parameters. The density is denoted by ρ, the flow velocity vector $\vec{u}$, the pressure p, and the shear stress tensor $\widetilde{\tau}$. Additional accelerations, such as gravitation, are considered in variables $\vec{f}$, specific internal energy e, specific enthalpy h, and Fourier's law of heat conduction $-\lambda \nabla T$. Furthermore, the RANS averaging, the transport equations of the $k-\varepsilon$ turbulence model, and other additional equations, such as the incompressible ideal gas law, are considered.

Because an exchange of mass, momentum, and energy is not considered, the Lagrangian equations can be highly simplified. The particle inertia can be written as in Ref. 31,

$$\frac{d\vec{u_P}}{dt} = \frac{3}{4}\frac{\rho_F}{\rho_P d_P} C_{drag}(\vec{u_F} - \vec{u_P})|\vec{u_P} - \vec{u_F}| + \vec{a}, \tag{7}$$

$$\frac{d\vec{s_P}}{dt} = \vec{u_P}, \tag{8}$$

with diameter d and drag coefficient C_{drag}, which is calculated using the spherical drag law. Index P represents particle parameters. All other additional accelerations, such as the Saffman lift force and gravitation in this case, are represented by $\vec{a}$. The vector $\vec{s}$ represents the position of the particle.

2. Discrete phase model

In this parameter study, a steady particle tracking based on a fixed steady airflow is solved with ANSYS Fluent. Due to the low mass fraction, the one-way-coupling is applied. Nevertheless, a two-way-coupling is activated to use further result variables. The influence of the particles on the flow is prevented by calculating the steady-state flow solution first without particles. Then, the Navier–Stokes equations are deactivated, and one Lagrangian iteration is calculated separately.

In a pre-analysis, it was examined whether the evaporation of the water component of the particles has to be considered for the simulation. A mass fraction of about 10.4% NaCl and 89.6% water is assumed.[1] According to the settings of Feng *et al.*,[1] the initial droplet diameters are fixed at 2 μm, which represents the smallest droplet diameter in their study. Compared to the aerosol particle diameter distribution used in this study, this represents a larger particle with a corresponding long evaporation time. An initial relative humidity of 0% is defined in the domain for the pre-analysis. The results show that the liquid water only exists for an average time of 0.024 s before it is completely evaporated. During this time, the particle trajectories travel about 1 mm. The range of influence of the gaseous water due to diffusion is limited to about 80 cm. In the following simulations, evaporation effects are neglected, and only solid particles are emitted directly from the particle source.

3. Inert particle setup

The inert particles of solid sodium chloride are injected in a 60° cone shape. The injection occurs at a spatial radius of 0.01 m. The initial velocity of the particles is set to 0.47 m/s at a total flow rate of $8.625 \cdot 10^{-10}$ kg/s. The activation of the Saffman law allows lift forces in shear flows. Based on the measured particle size distribution, the analytic Rosin–Rammler distribution is used to adjust the particle diameters in the simulations to the experimental diameter distribution of the aerosol generator. This distribution is defined by the following parameters: minimal diameter, $0.19 \cdot 10^{-6}$ m; maximum diameter, $9.65 \cdot 10^{-6}$ m; mean diameter, $3.57 \cdot 10^{-6}$ m; and a spread parameter, 1.90. A stochastically random walk model of 10 leads to a total number of 10 000 trajectories that are calculated in a simulation. The maximum number of steps of 100 000 and a step length factor of 5 define the tracking parameters and the abort criteria if a particle stream does not reach a target boundary. For the calculation of the trajectories, an automatic adaptive time step is used. It is assumed that particles stick on all solid surfaces due to van der Waals forces.[21] Complete reflection and reentry of particles at the door gap and pressure side of the purifier are assumed. Particles can escape the domain at the intake of the air purifier.

4. CFD setup

The turbulence modeling is performed using the $k-\varepsilon$ realizable model with the Menter–Lechner wall treatment. It is assumed that the airflow in the room is steady. According to the incompressible ideal gas law, thermally induced buoyancy flows are considered. At low temperatures and normal room temperature, heat transfer by radiation can be neglected.[32] According to DIN EN 13779,[33] persons in the classroom represent a heat source with a heat flux of $\dot{q}_{Person} = 41,67\ \mathrm{W/m^2}$. In winter, the window surface temperature cools down and radiators are used.[34] The thermal power loss of the air purifier is adapted according to the power level of the fan. The equations are solved in a coupled scheme. The Navier–Stokes equations are discretized with a second order method in space. The two additional transport equations for the turbulence modeling are solved with first order accuracy.

B. Case studies

Due to the steady-state flow simulation, particle charging and decaying phases cannot be considered as in the experiments. Based on a steady-state flow field, the Lagrangian solution still provides time-dependent information and allows for a validation by comparison with the experimental results. First, simulations are performed to validate the setup and to compare the results with experimental data. When investigating the influence of the location of the air purifier and particle source on the local aerosol concentration, the simulations are performed according to the experiments. In addition, the visualization of the room air flow will provide further references for the operating conditions of air purifiers. A comparison of summer and winter cases shall determine the influence of cold window surfaces and warm radiators.

IV. RESULTS AND DISCUSSION

A. Experimental results

The experimental results are split up into the validation of the measurement method, the decay rate comparison of the high-end OPC and low-cost particle sensors, the evaluation of the position and orientation of the air purifier, and the influence of the position of the aerosol particle source on local exposure.

1. Validation of instruments and measurement method

In order to validate the measurement method, five low-cost particle sensors are placed along a grid at the face-height of a single thermal dummy and one high-end OPC is placed at the table height for comparison (see Fig. 2).

The air purifier is positioned in the south-western corner of the classroom and oriented so that the outlet points toward the front of the room (SW-S). The aerosol particles are emitted at the back of the room near the air purifier (position 80; see Fig. 1). After 4 min of measuring the ambient particle concentration, the atomizer (3.5 bar; 16 wt. % NaCl solution) and air purifier (ACH: 5) are turned on. After 20 min of charging the room with particles, the atomizer is shut off and the air purifier kept running for further 20 min. To distinguish between potential spatial concentration differences, in further experiments, the central sensor unit is fixed in place, while the surrounding sensors are cycled around the center point (experiments V1–V4).

The PM1 dose at each point is set in relation to the center point value. A comparison of the PM1 doses at each measuring point (Fig. 3, right) and the PM1 dose measured by each

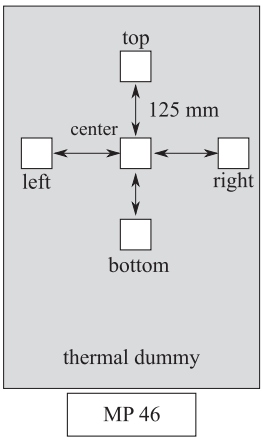

FIG. 2. Four low-cost particle sensors are cycled around a central sensor at the face-height of a thermal dummy. A high-end OPC on the table is used as a reference.

device relative to the center point (Fig. 3, left) shows a consistent offset between the single devices independent of their respective location. The high-end OPC (MP 46) consistently measures a 20%–30% higher PM1 dose. This is due to the wider measuring range and a more precise measurement at high particle counts (>5000 P/cm^3). Although the exact PM1 mass concentration is subjected to uncertainties due to the varying measurement precision of the low-cost and high-end sensors, the reduction in the relative PM1 exposure at either the table height or face height and the decay rate at each measurement point can be used to evaluate the efficiency of the air purifier depending on the operating parameters.

2. Decay rate of low-cost and high-end sensors

Figure 4 shows the temporal PM1 mass concentration curve of an exemplary validation experiment. Regression coefficients $R^2 > 0.99$ show a high correlation between the fitted decay curves and measured data. The decay rate at a single point in the room at an ACH of 5 and 10 are (0.092 ± 0.001) min^{-1} and (0.188 ± 0.002) min^{-1}, respectively. In this case, 50% of the initial particle concentration decay after (7.52 ± 0.09) min at an ACH of 5. Increasing the ACH to 10 gives a half-life time of (3.63 ± 0.04) min, while 99% of the initial particle concentration decays after (24.6 ± 0.7) min. Using Eq. (1), with the natural decay rate of $k_{natural}$ = 0.008 min^{-1} and the room volume of 250 m^3, the resulting CADRs are calculated to be 1260 and 2700 m^3/h.

3. Evaluation of the position and orientation of the air purifier

The influence of the position and orientation of the air purifier on the distribution and decay of the aerosol particles was evaluated by comparing the PM1 dose at four measurement points using the high-end OPCs. In Fig. 5 (left), the PM1 dose at each measurement point is shown. The location of the air purifier has a noticeable impact on the distribution of the emitted particles. While in the absence of an air purifier, the emitted particles initially follow the thermally induced air flow by the measurement point MP 58 (located between the particle source in the middle of the room and the window front), operating the air purifier leads to an increased PM1 concentration at measurement points close to the intake. For positions NE and N, this is MP 58. Positions NW and SW show the increased concentration at points MP 86 (back of the room) and MP 52 (near wall). In the case of NE-E, the emitted particles traveled to the intake without passing by the OPC, leading to a minimal PM1 dose measured in this setup. This example clarifies that a high spatial resolution is necessary especially during the charging phase where it cannot be assumed that the particle concentration is homogeneous throughout the room. In order to evaluate the setup parameters of the air purifier, the calculated PM1 doses were averaged within three setup categories: (I) the air purifier outlet is obstructed (oriented in such a way that the outlet points toward the wall or window), (II) the outlet is unobstructed (oriented in such a way that the outlet points freely into the room), and (III) the outlet and intake are

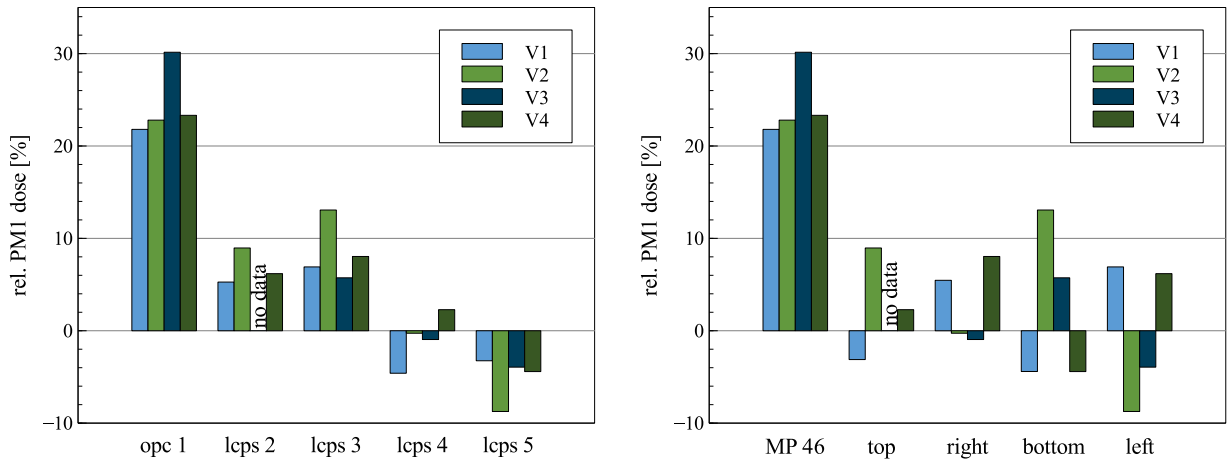

FIG. 3. Left: relative PM1 dose in relation to the center measurement point by the device. Right: relative PM1 dose measured by the location.

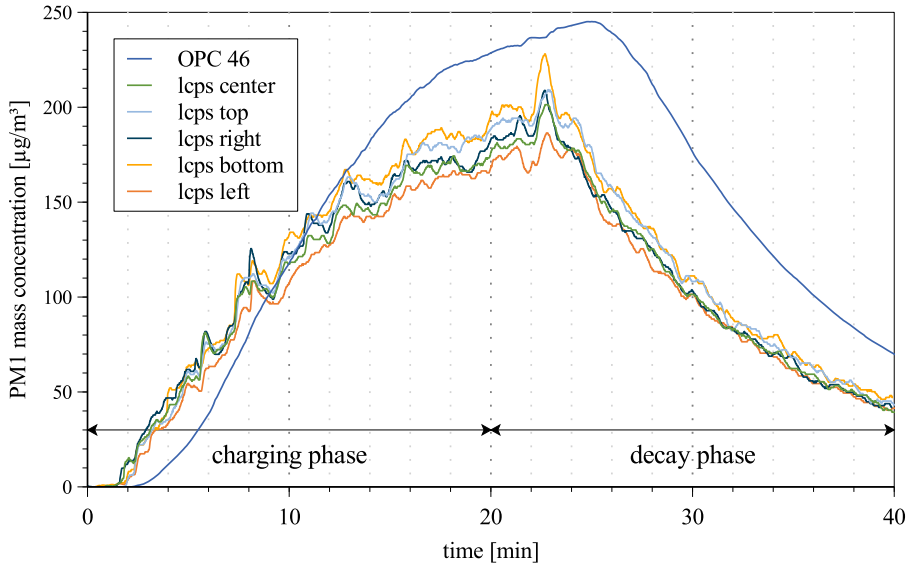

FIG. 4. Temporal PM1 mass concentration of an exemplary validation experiment showing the charging and decay phases.

obstructed (oriented in such a way that both the outlet and the intake are obstructed by either a wall or a window). Figure 5 (right) shows the average PM1 doses for categories I, II, and III over both charging and decay phases and split up into each phase.

In all cases, the air purifier reduces the particle load compared to the natural decay. Setting up the air purifier by obstructing the outlet leads to an average 70% reduction of the total PM1 dose over the charging and decay phases. By pointing the outlet stream unobstructed into the room, the PM1 dose is only reduced by an average of 58%. This is attributed to the outlet stream distributing the emitted aerosol particles throughout the room during the charging phase rather than depositing them. Obstructing the outlet and the intake of the air purifier is particularly disadvantageous, leading to an average PM1 dose reduction of only 30% while showing a PM1 dose comparable to the absence of the air purifier during the charging phase. It can be concluded that the orientation of the air purifier has a significant impact on the efficiency of the reduction of the airborne particulate matter. In this case, obstructing the outlet stream reduces the distribution of the aerosol particles throughout the room. This ensures that the air purifier is employed at maximum efficiency.

4. Influence of the aerosol particle source on local exposure

Derived from the results of the first experimental setup, four cases are investigated further (SW-W, SW-S, SW-N, and no air purifier). The new experimental setup includes nine thermal dummies equipped with low-cost sensors at the face-height and varying positions of the aerosol particle source (see Fig. 6). The PM1 dose over the course of the experiment is set in relation to the PM1 dose measured using no air purifier (see Fig. 7, left).

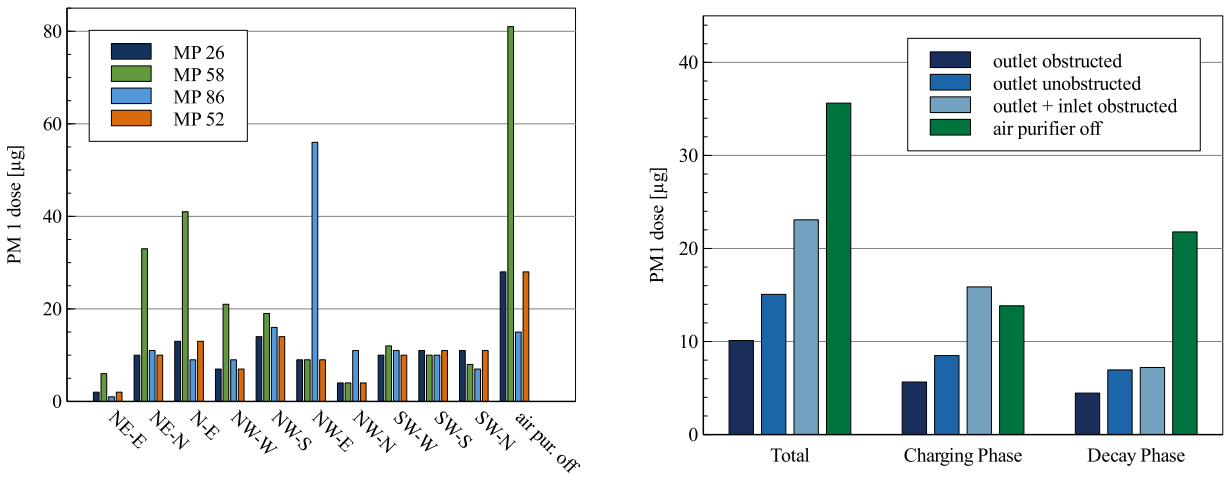

FIG. 5. Left: PM1 dose at each measurement point for all investigated setup parameters at an ACH of 5. Right: averaged PM1 dose by the setup category at an ACH of 5.

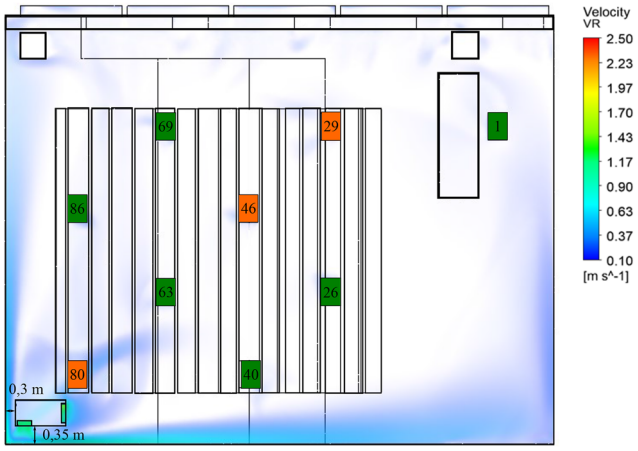

FIG. 6. Experimental setup showing the location of the air purifier, aerosol source positions (orange), measurement points (orange and green), and an air velocity larger than 0.1 m/s for position SW-W at an ACH of 5.

Overall, the use of the air purifier decreases the PM1 dose independently of the aerosol source compared to no air purifier (see Fig. 7, right). The highest reduction was achieved with the outlet directed at the wall (setup parameter, SW-W), decreasing the PM1 dose throughout the room on average by 75% independently of the aerosol source position. This is slightly higher than the reduction determined in the first experimental setup due to the fact that emitting particles near the intake leads to an overall reduction of well above 80%. SW-N decreases the PM1 dose throughout the room on average by 61%. In this worst-case scenario (both the intake and outlet are obstructed), the aerosol particles are emitted from seat 29 at a significant distance to the air purifier. Further dependency on the aerosol source position is not investigated. The last case with an unobstructed intake and outlet (SW-S) decreases the PM1 dose throughout the room on average by 61%. This is very close to the 58% reduction of the PM1 particle concentration measured in the first experimental setup for the unobstructed intake and outlet. Regarding the charging phase, SW-S leads to localized increases in the PM1 dose compared to no air purifier, further indicating that an unobstructed outlet negatively effects the removal of the aerosol particles. SW-W holds up to be the best setup case, showing the lowest increase in the PM1 dose during the charging phase independently of the location of the aerosol source and indicating that obstructing the outlet air flow is a viable strategy in preventing the distribution of particles throughout the room.

B. Numerical results

1. Validation of the numerical model

The impact of the mesh on the results of the CFD simulation is investigated. Starting from a fine mesh, the grid is coarsened and the resulting differences are evaluated.

Using a fine and medium mesh, similar vortex structures can be seen at a head height of 1.7 m (see Fig. 8). In contrast, when using the coarse mesh, different flow vortices occur in the center of the room. Even though the faster flow velocity larger than 0.1 m/s of all mesh variants corresponds very well to the results using the fine mesh, different aerosol particle dispersion occurs. The particle trajectories take different paths because of the slow flow vortices in the center of the room where the particles are injected. The medium mesh settings are used as a compromise between computational duration and accuracy.

2. Validation using steady particle tracking

A validation of the simulation results is done based on the stationary particle simulation since this is also used in the simulation study. Here, temporal information is only available in the Lagrangian phase.

After 60 s, the particles have barely dispersed. No measuring device should react to the turned-on aerosol source [see Fig. 9(a)]. After about 2 min, the particles have arrived at MP58 and MP86. MP58 is exposed to the most particles [see Fig. 9(b)]. MP26 and MP52 do not show any measurement data yet. After about 3 min,

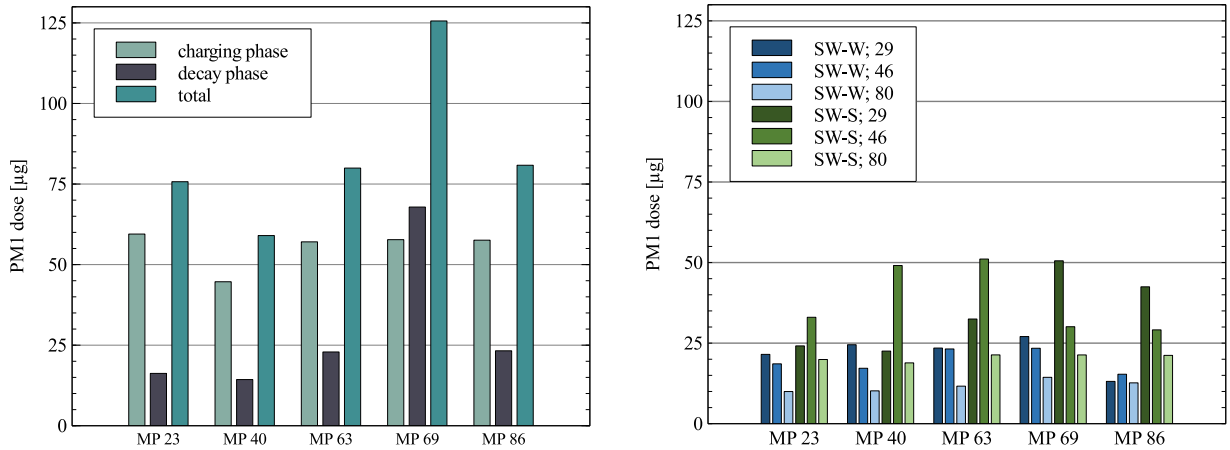

FIG. 7. Left: PM1 dose at the face height in the absence of the air purifier. Right: PM1 dose at the face height for positions SW-W and SW-S depending on the aerosol source (29, 46, and 80) at an ACH of 5.

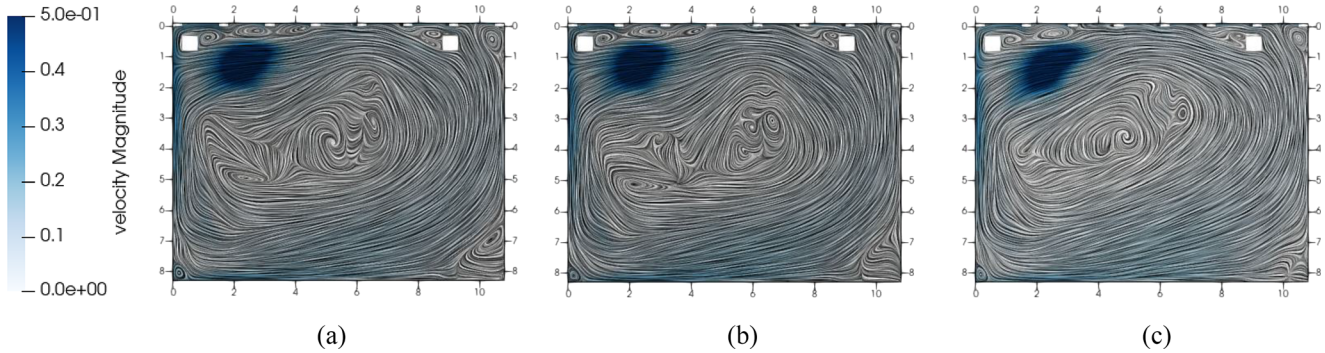

FIG. 8. Comparison of vortex structures in slow flow regions on different meshes. (a) Fine mesh, (b) medium mesh, and (c) coarse mesh.

the particle trajectories pass MP52 [see Fig. 9(c)]. At MP26 near the placement of the air purifier, the first particles from the aerosol generator are measured only after 4 min [see Fig. 9(d)]. This matches to the experimental data in Fig. 10.

3. Validation using unsteady particle tracking

A transient particle simulation can offer further information for the validation of the simulation settings to the experimental measurement results. To evaluate the mass concentration spatially and temporally, control volumes have to be defined according to the position of the OPCs.

The order of magnitude and the time evolution of the mass concentration at the control volumes match to the experimental data at the measurement locations.

4. Influence of the air purifier and particle source on local particle exposure

The analysis of the air flow at different positions of the air purifier already gives an insight into the aerosol distribution. According to DIN EN ISO 7730, a maximum average air velocity of 0.24 m/s is specified for classrooms.[35] In all cases, the flow velocity at the occupied seats is low enough not to cause thermal discomfort (see Fig. 11).

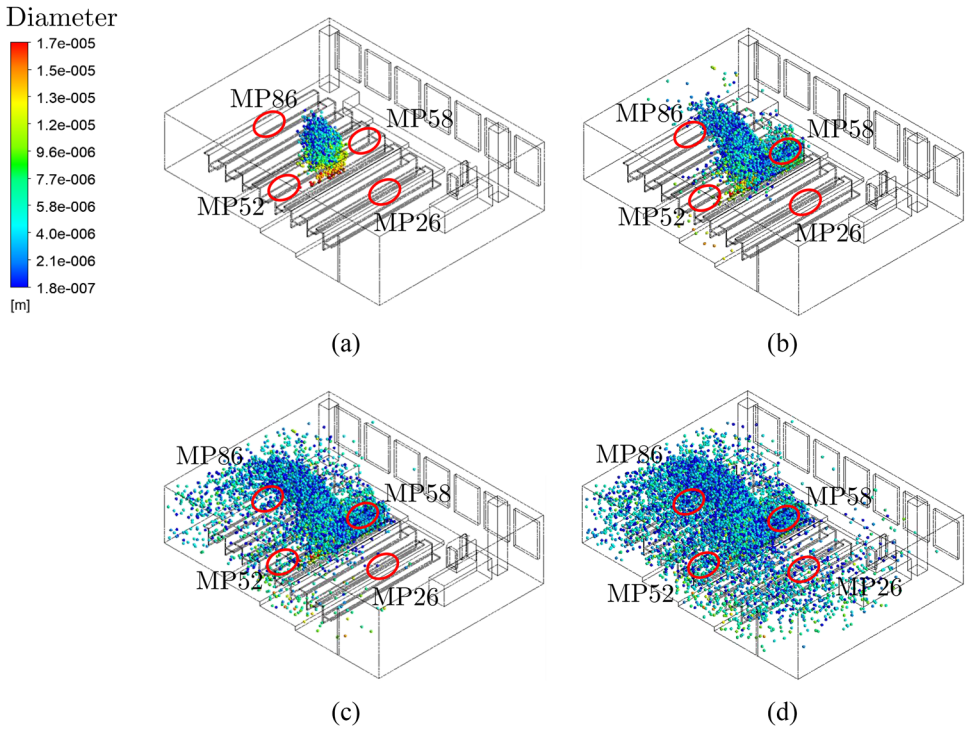

FIG. 9. Dispersion of Lagrange particles using steady particle tracking for validation with measurement data. (a) t = 60 s, (b) t = 120 s, (c) t = 180 s, and (d) t = 240 s.

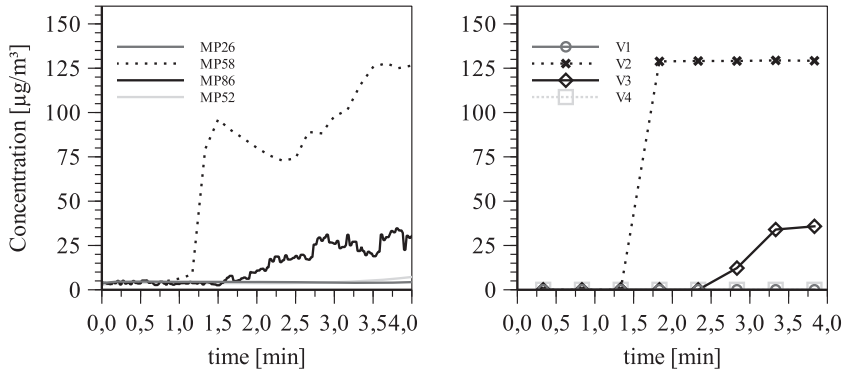

FIG. 10. Comparison of the particle mass concentration determined experimentally (left) and unsteady simulation (right) at four different measurement locations at an ACH of 5.

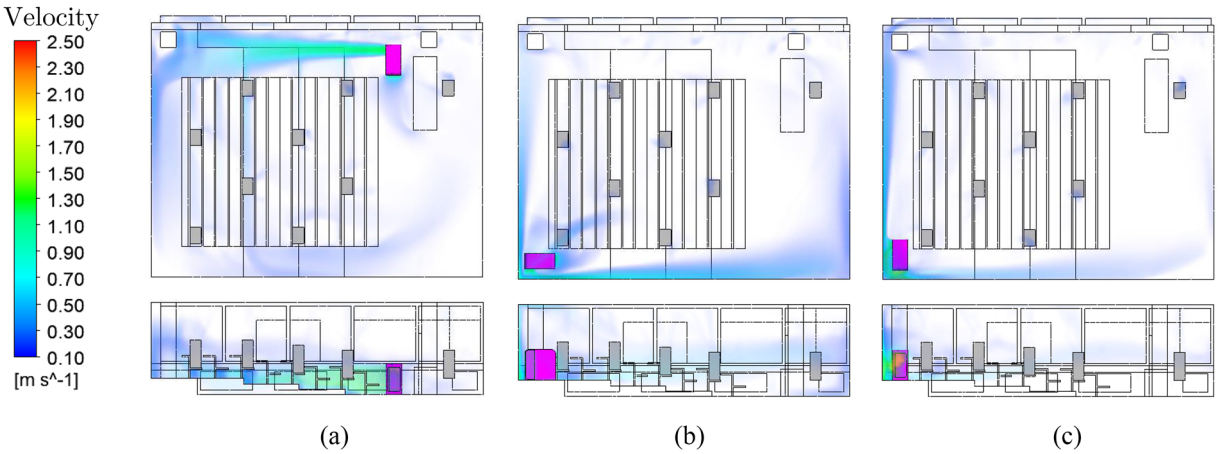

FIG. 11. Comparison of different air purifier positions and air velocities at an ACH of 5. (a) Position NE-N, (b) Position SW-W, (c) Position SW-N.

The fates describe the number of particle streams arriving at a defined target boundary. The different labels represent different particle source positions. The data series represent the different locations of the air purifier in Fig. 12. Particles that reach the air purifier can be removed from the ambient air. This reduces the amount of potentially infectious particles. The plotted data show the relative number of particle streams that are collected in the filter at an ACH of 5, allowing us to compare different positions and orientations of the air purifier at the same filter volume flow.

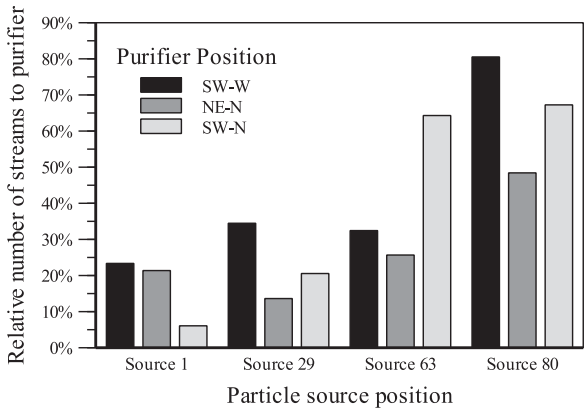

FIG. 12. Particle fates for different purifier positions and different particle source positions at an ACH of 5.

In air purifier position SW-N, it is noticeable how strongly the number of filtered streams depends on the source position. In the worst case, only about 5% of the particle streams reach the filter. Due to this strong dependence of the source position, the purifier position SW-N is not recommended. Position NE-N shows the best uniformity of the number of filtered streams. However, this is at a generally low level so that on average only about 28% of the injected particle streams arrive at the air purifier. Position SW-W achieved the best results in this comparison. On average, about 40% of the emitted particle streams reach the room air purifier. In the worst case, still about 25% of the particle streams are removed by the filter. The positioning of the room air filter with outflow against the wall and intake in the direction of the room interior shows the best results in this simulation comparison. The visualization of the mass concentration allows qualitative evaluations of the particle paths from the injection to their target boundary. A column represents one particle source position and allows for a comparison of the different locations of the air purifier in different rows in Fig. 13.

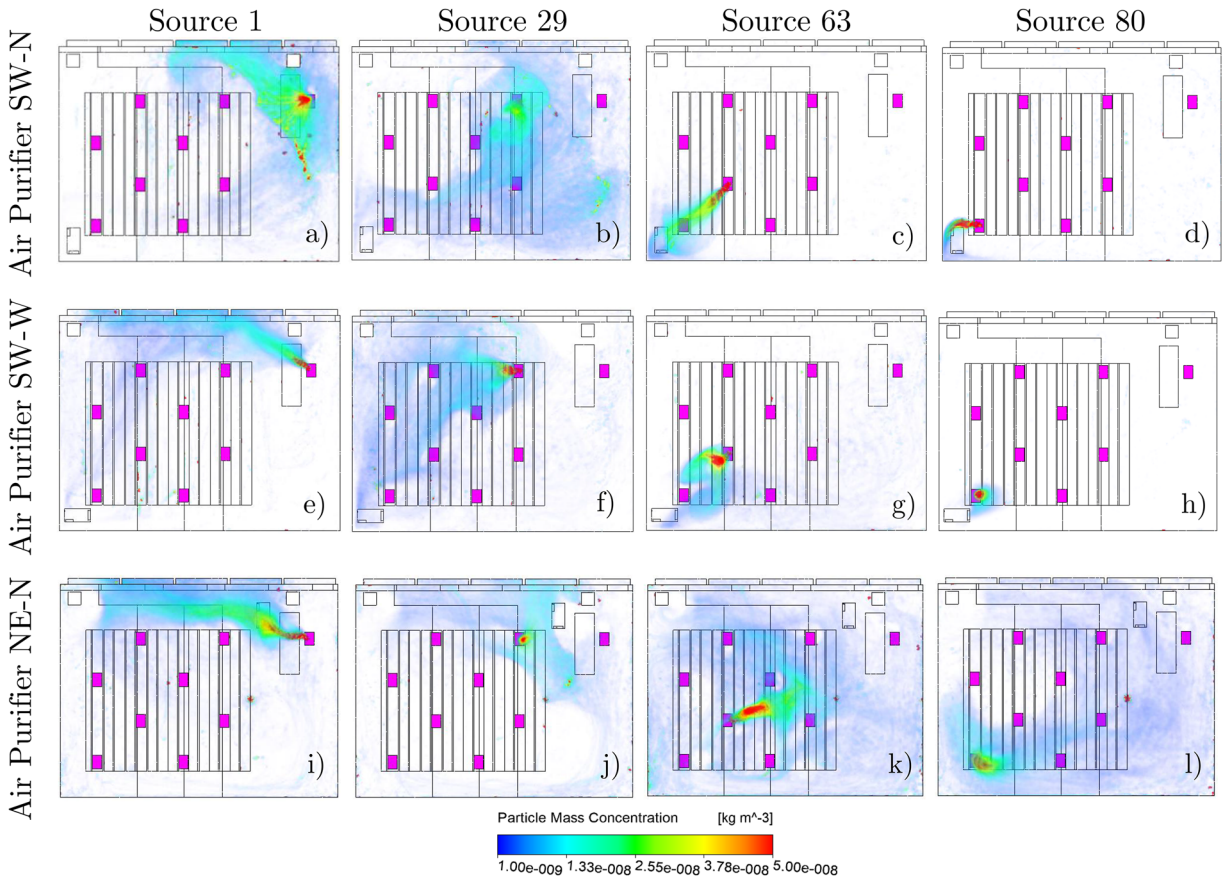

FIG. 13. Particle concentration of different air purifier positions and particle source positions at an ACH of 5. (a)–(d) Air purifier position SW-N with the aerosol source positions 1, 29, 63, and 80. (e)–(h) Air purifier position SW-W. (i)–(l) Air purifier position NE-N.

5. Extended case studies

As an extension of the numerical study, the flow velocity at different ACHs and the differences in buoyancy flows in summer and winter will be investigated.

6. Air velocity for different ACHs

The zone of influence of the intake of the air purifier is significantly smaller than the pressure side area. This value is exceeded at the person seats when the air purifier operates at the highest level (see Fig. 14). At an ACH of 5, these comfort limits are just fine in the seating areas. This level represents the maximum performance of the room air filter in this room and this positioning without causing discomfort to the persons due to excessive air velocities. Operation of the room air filter at an ACH of 5 is recommended in this room to achieve the best possible compromise between comfort due to air velocity and filter volume flow. The air purifier has to be oriented in such a way that the outflow area is not directed toward occupied seats. In addition, with the variation in the ACH, it can be shown that the duration of the particle movement from the source to the air purifier decreases with a higher flow rate. Depending on the air change rate, redirecting particles to the air purifier reduces the possible infectious particle streams by more than 50% (see Fig. 15).

7. Summer vs winter air flow

Using the incompressible ideal gas law, the air density can change due to local temperature differences. The density differences lead to buoyancy forces. In Fig. 16, the vertical velocity (v in the positive Y-direction) is shown. The difference of summer and winter simulation is mainly noticeable at the window side. The cold window glass in winter leads to sinking air flows. Directly below the window is the radiator, which causes upward flows. At the height of the window sill, these descending and ascending streams intersect and lead to a lateral deflection of the heating flow toward the interior of the room. However, the area of influence of the heating flow is locally limited to about one m.

V. LIMITATIONS OF THE PRESENTED APPROACH

While the PM1 dose is used to evaluate the efficiency of the air purifier, it is unlike the inhaled particulate matter responsible for airborne transmission. First, this is due to inhaled particles being

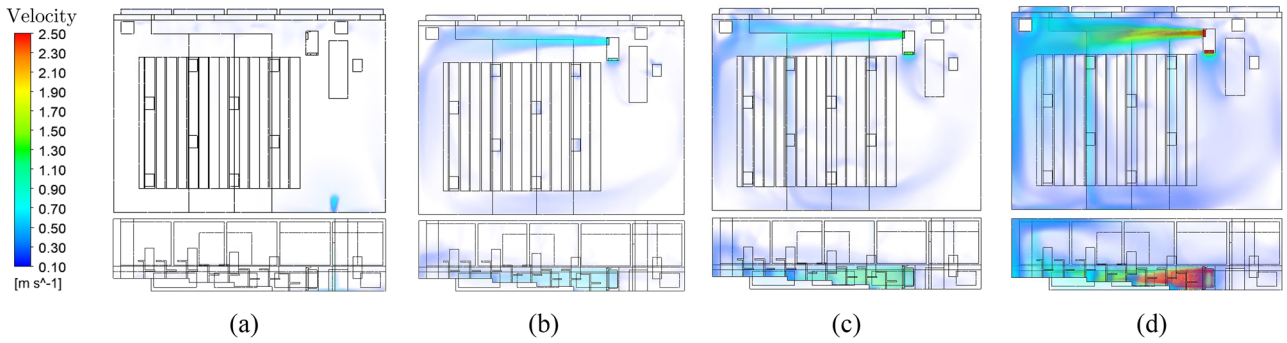

FIG. 14. Air velocity (NE-N) at different ACHs. (a) ACH = 0, (b) ACH = 3, (c) ACH = 5, (d) ACH = 10.

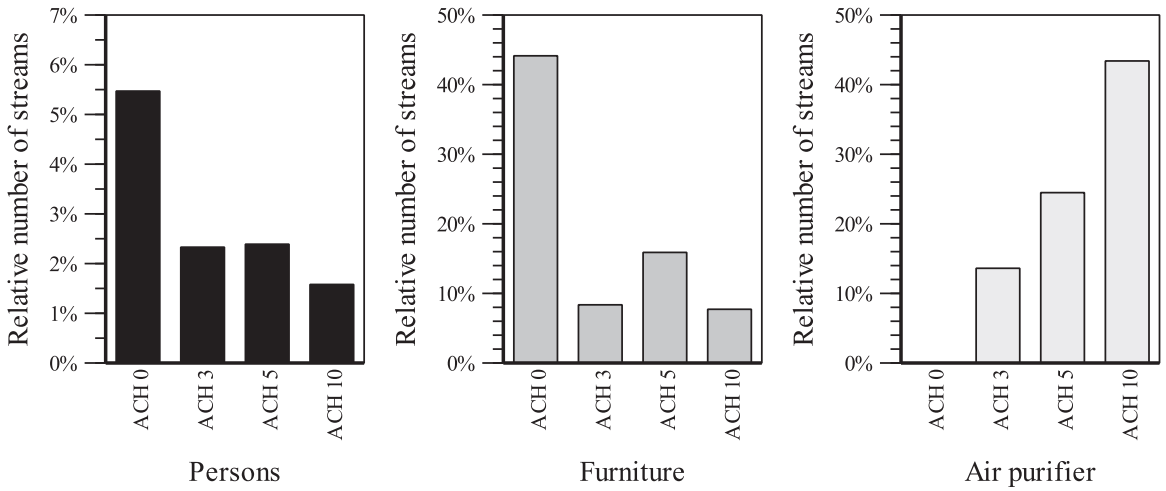

FIG. 15. Comparison of particle fates at different ACHs.

deposited in the lungs and therefore removed from further circulation. However, assuming an average relaxed breathing rate of 8 L/min and lungs with a filter efficiency of 100%, the combined CADR of 80 occupants amounts to 38.4 m^3/h. Even at full occupancy, the CADR by lung deposition is negligibly small compared to the CADR of an air purifier. Second, the actual exposure to virus-laden droplets is far lower than the exposure measured in this study. For this reason, no direct infection risk was calculated, but rather the relative infection risk connected to the optimized operating parameters of the air purifier was evaluated. In real-world applications, the HVAC system is likely to be running, influencing the distribution and decay of the particle concentration. Furthermore, the examined cases did not include dynamic processes, such as moving particle sources and varying source strength (through coughing, talking, etc.). Since most air purifiers on the market today are highly distinguishable in their design regarding the location of the intake and outlet, this is a highly specific case from which no generalization of the observed phenomenon to all types of air purifiers can be made. Although the low-cost particle sensors have a much lower resolution and a narrower measurement range compared to the high-end OPCs, the validation experiments showed that the decay rate is highly comparable to that of the latter devices. Since the high-end OPCs measure considerably more PM1 mass concentration over the course of the experiment, the efficiency of the air purifier was evaluated either by comparing the low-cost particle sensor or high-end OPC data. In order to push the particle size distribution into the

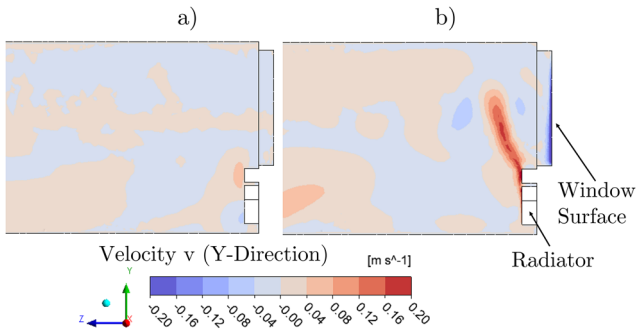

FIG. 16. Comparison of summer (a) and winter (b) air flows near windows and radiator. (a) Summer and (b) Winter.

measurement range of the low-cost particle sensors, the mass concentration of the saline solution was raised from 2.5 wt. % in the first experimental setup to 16 wt. % in the second. This raised the median particle diameter $x_{50,0}$ from 0.25 to 0.34 μm. The experiments were carried out over a substantial period in winter going into spring. The ambient conditions changed accordingly and influenced parameters such as outside temperature and relative humidity, which will influence the thermal convection of particle exposure throughout the room. Furthermore, the investigation focuses on a single room and the transferability to other rooms is yet to be investigated.

The most critical point is the assumption that particle fates correlate with the infection risk. This correlation has not been proven and is an assumption. In addition, it is assumed that each stream has the same potential for infection. Obviously, not only the destination of the particle streams is relevant for the infection risk. Particles can be infectious on their path between injection and destination boundary. For this reason, the particle mass concentration was calculated. From the experimental results, it is known that the particle mass concentration with the build-up phase and decay phase is strongly time-dependent. The numerical result is only available as stationary averaged values in time. Therefore, it can only be used as a subjective evaluation criterion. A limited number of 10 000 trajectories are calculated in the simulation, although in reality the number of particles is essentially higher. Another aspect is differences of the numerical model from reality. First, the geometric model is highly simplified. In addition, the real boundary conditions of the room are difficult to detect and to transfer into the simulation boundary conditions.

VI. CONCLUSION

In this work, we have studied the influence of the position and orientation of an air purifier on the aerosol particle concentration in a lecture hall and identified preferable cases with respect to a low aerosol exposure of persons present in the room. Specifically, we have set up a PM1 sensor network consisting of 12 sensors exactly at the locations where particles may be inhaled and included the influence of thermal buoyancy by mimicking the effect of persons present in the room using thermal dummies. We investigated both the charging phase where the air purifier fights against a source (the "infected person is in the room") and the decay phase (the "infected person has left the room"). Furthermore, we validated a CFD model based on the measurements in order to study particle fates and to allow for the investigation of situations, which can hardly or not be considered experimentally. Overall, the results stress that filtration is an effective means of reducing aerosol particle concentrations. The measurements suggest that a blowout against the wall may be particularly advantageous in order to avoid an increase in the local particle concentration at the locations where persons breathe after turning on the air purifier. In turns out that the air purifier can very effectively reduce aerosol particle concentrations in a combined loading and decay scenario by 86% using a good orientation with the obstructed outlet and by 61% in an unfavorable orientation and position. The CFD simulations suggest that an additional effect of risk mitigation is the fact that the air purifier reduces the deposition of aerosol particles on critical surfaces (persons and furniture).

However, it needs to be stressed that the aerosol dose and particle fates may differ from the actual infection risks due to system-inherent differences, such as the fact that inhaled particles are removed in reality but remain within the system in the models and in the experiments. Further work needs to be done to provide insight into the fact how the specific flow configuration influences the results. Therefore, this study should be extended taking into account different air purifier devices. In addition, it needs to be investigated to which extend the results obtained depend on the specific geometry of the lecture hall and how far they can be generalized.

ACKNOWLEDGMENTS

This research was partly funded by the Ministry of Science, Research and the Arts (MWK) of the State of Baden-Württemberg in the frame of the special funding track COVID-19 research, part of the measures for fighting the SARS-CoV-2 pandemic in the frame of medical research.

AUTHOR DECLARATIONS

Conflict of Interest

The authors declare that there is no conflict of interest.

DATA AVAILABILITY

The data that support the findings of this study are available from the corresponding author upon reasonable request.

REFERENCES

[1] Y. Feng, T. Marchal, T. Sperry, and H. Yi, "Influence of wind and relative humidity on the social distancing effectiveness to prevent COVID-19 airborne transmission: A numerical study," J. Aerosol Sci. **147**, 105585 (2020).

[2] R. de La Fuente Briones, *Argentum 47: So hilft Silber gegen das Corona-Virus* (BoD-Book on Demand, Nordersteadt, Germany, 2020).

[3] C. Spindler, Charakterisierung Biogener Sekundärer Organischer Aerosole mit Statistischen Methoden: Zugl.: Wuppertal, Univ., Diss., 2010, Schriften des Forschungszentrums Jülich Reihe Energie & Umwelt, Vol. Bd. 63 (Forschungszentrum Jülich, Jülich, 2010).

[4] A. Sharma, R. Goyal, and R. Mittal, *Indoor Environmental Quality: Select Proceedings of the 1st ACIEQ*, 1st ed., Lecture Notes in Civil Engineering (Springer Singapore and Imprint: Springer, Singapore, 2020).

[5] M. Kriegel, U. Buchholz, P. Gastmeier, P. Bischoff, I. Abdelgawad, and A. Hartmann, "Predicted infection risk for aerosol transmission of SARS-CoV-2," medRxiv preprint (published online).

[6] American Society of Heating, Refrigerating and Air-Conditioning Engineers, Ventilation of health care facilities, 2017.

[7] DIN EN 16798, Energetischebewertung von gebäuden - lüftung von gebäuden, 2017.

[8] J. Szabadi, J. Meyer, M. Lehmann, and A. Dittler, "Simultaneous measurement of the temporal and local development of particle concentrations of different source strengths in closed indoor rooms applying a highly efficient mobile air filter," J. Aerosol Sci. **160**, 105906 (2022).

[9] C. J. Kähler, T. Fuchs, and R. Hain, "Können mobile raumluftreiniger eine indirekte SARS-CoV-2 infektionsgefahr durch aerosole wirksam reduzieren?" (preprint).

[10] S. Burgmann and U. Janoske, "Transmission and reduction of aerosols in classrooms using air purifier systems," Phys. Fluids **33**, 033321 (2021).

[11] J. Curtius, M. Granzin, and J. Schrod, "Testing mobile air purifiers in a school classroom: Reducing the airborne transmission risk for SARS-CoV-2," Aerosol Sci. Technol. **55**, 586–599 (2021).

[12]S. Ham, "Prevention of exposure to and spread of COVID-19 using air purifiers: Challenges and concerns," Epidemiol. Health **42**, e2020027 (2020).
[13]M. A. Kohanski, L. J. Lo, and M. S. Waring, "Review of indoor aerosol generation, transport, and control in the context of COVID-19," Int. Forum Allergy Rhinol. **10**, 1173–1179 (2020).
[14]M. Küpper, C. Asbach, U. Schneiderwind, H. Finger, D. Spiegelhoff, and S. Schumacher, "Testing of an indoor air cleaner for particulate pollutants under realistic conditions in an office room," Aerosol Air Qual. Res. **19**, 1655–1665 (2019).
[15]Association of Home Appliance Manufacturers, *Method for Measuring Performance of Portable Household Electric Room Air Cleaners* (ANSI, 2020).
[16]X. Chen, Y. Feng, W. Zhong, and C. Kleinstreuer, "Numerical investigation of the interaction, transport and deposition of multicomponent droplets in a simple mouth-throat model," J. Aerosol Sci. **105**, 108–127 (2017).
[17]Á. Farkas, F. Lizal, J. Jedelsky, J. Elcner, J. Karas, M. Belka, O. Misik, and M. Jicha, "The role of the combined use of experimental and computational methods in revealing the differences between the micron-size particle deposition patterns in healthy and asthmatic subjects," J. Aerosol Sci. **147**, 105582 (2020).
[18]X. Xie, Y. Li, A. T. Y. Chwang, P. L. Ho, and W. H. Seto, "How far droplets can move in indoor environments—Revisiting the wells evaporation-falling curve," Indoor Air **17**, 211–225 (2007).
[19]J. K. Mutuku, W.-C. Hou, and W.-H. Chen, "An overview of experiments and numerical simulations on airflow and aerosols deposition in human airways and the role of bioaerosol motion in COVID-19 transmission," Aerosol Air Quality Res. **20**, 1172–1196 (2020).
[20]T. Dbouk and D. Drikakis, "On airborne virus transmission in elevators and confined spaces," Phys. Fluids **33**, 011905 (2021).
[21]M. Abuhegazy, K. Talaat, O. Anderoglu, and S. V. Poroseva, "Numerical investigation of aerosol transport in a classroom with relevance to COVID-19," Phys. Fluids **32**, 103311 (2020).
[22]B. Gorbunov, "Aerosol particles generated by coughing and sneezing of a SARS-CoV-2 (COVID-19) host travel over 30 m distance," Aerosol Air Quality Res. **21**, 200468 (2021).
[23]S. Bathula, S. Anand, T. Thajudeen, Y. S. Mayya, P. Chaudhury, and C. Shashank, "Survival of expiratory aerosols in a room: Study using a Bi-compartment and Bi-component indoor air model," Aerosol Air Quality Res. **21**, 200547 (2021).
[24]O. V. Pyankov, S. A. Bodnev, O. G. Pyankova, and I. E. Agranovski, "Survival of aerosolized coronavirus in the ambient air," J. Aerosol Sci. **115**, 158–163 (2018).
[25]N. Rezaei, M. Jafari, A. Nazari, S. Salehi, F. Talati, R. Torab, and R. Nejad-Rahim, "A novel methodology and new concept of SARS-CoV-2 elimination in heating and ventilating air conditioning systems using waste heat recovery," AIP Adv. **10**, 085308 (2020).
[26]Y. Feng, J. Zhao, M. Spinolo, K. Lane, D. Leung, D. Marshall, and P. Mlinaric, "Assessing the filtration effectiveness of a portable ultraviolet air cleaner on airborne SARS-CoV-2 laden droplets in a patient room: A numerical study," AerosolAir Quality Res. **21**, 200608 (2021).
[27]DIN EN 1822-1, Schwebstofffilter (epa, hepa und ulpa)—Teil 1, 2019.
[28]Gesellschaft für Aerosolforschung e.V., Position paper of the gesellschaft für aerosolforschung on understanding the role of aerosol particles in SARS-CoV-2 infection.
[29]A. Faghri and Y. Zhang, *Fundamentals of Multiphase Heat Transfer and Flow*, 1st ed. (Springer International Publishing and Imprint: Springer, Cham, 2020).
[30]S. Lecheler, *Numerische Strömungsberechnung: Schneller Einstieg in ANSYS CFX 18 durch einfache Beispiele*, 4th ed. (Springer Vieweg, Lehrbuch, Wiesbaden, 2018).
[31]A. D. Gosman and E. loannides, "Aspects of computer simulation of liquid-fueled combustors," J. Energy **7**, 482–490 (1983).
[32]W. Polifke and J. Kopitz, *Wärmeübertragung: Grundlagen, analytische und numerische Methoden*, 2nd ed., Maschinenbau (Pearson Studium, München, 2009).
[33]DIN EN 13779, Lüftungvon nichtwohngebäuden – allgemeine grundlagen und anforderungen für lüftungs -und klimaanlagen und raumkühlsysteme, deutsche fassung en 13 779, 2007, 2007.
[34]A. Jurelionis and E. Isevičius, "Cfd predictions of indoor air movement induced by cold window surfaces/vėsi lang pavirši sukeliamo oro judėjimo tyrimai pasitelkiant kompiuterinio modeliavimo metodus," J. Civ. Eng. Manage. **14**, 29–38 (2008).
[35]DIN EN ISO 7730, Ergonomie der thermischen umgebung – analytische bestimmung und interpretation der thermischen behaglichkeit durch berechnung des pmv- und des ppd-indexes und kriterien der lokalen thermischen behaglichkeit, 2005.